14

Flexible Electrically Conductive Films Based on Biocompatible Composite Material

© L.P. Ichkitidze,[1,2] K.D. Popovich,[1,2] V.V. Suchkova,[1,2] D.I. Ryabkin,[1,2] S.S. Hosseini,[3] V.A. Petukhov,[1] D.V. Telyshev,[1,2] S.V. Selischev,[1] A.Yu. Gerasimenko[1,2]

[1] Institute of Biomedical Systems,
National Research University of Electronic Technology „MIET“,
124498 Moscow, Zelenograd, Russia
[2] Institute for Bionic Technologies and Engineering,
Sechenov First Moscow State Medical University, Sechenov University,
119991 Moscow, Russia
[3] Department of Biomedical Engineering, North Tehran Branch,
Islamic Azad University,
Tehran, Iran
e-mail: leo852@inbox.ru, ichkitidze_l_p@staff.sechenov.ru

Received November 1, 2024
Revised November 1, 2024
Accepted November 1, 2024

Biocompatible composite materials based on carbon nanotubes contained in the matrix exhibit strain-resistive properties under deformation. The possibility of their use as a prototype of a tactile sensor was investigated. The layers in the matrix of microcrystalline cellulose and the filler of multi-walled carbon nanotubes served as a tactile sensitive element. Aqueous suspension of the composite material was applied on a substrate (thickness $30\,\mu$m) made of polyethylene with subsequent exposure of the sample to laser radiation. It is shown that the tactile sensitive element based on thin layers of composite (thickness $\leq 1\,\mu$m) exhibits the properties of a bipolar strain sensor, and thick layers (thickness $\geq 10\,\mu$m) exhibit the properties of a unipolar strain sensor. It is found that tensoresistive measurements allow to fix the pressure $\sim 0.2-20$ Pa, which corresponds to the order of tactile sensitivity of human fingers. The prospect of using the obtained results in flexible electronics or for creation of T-sensors and electronic skin (e-skin) is considered. The work was carried out within the framework of the state assignment of the Russian Ministry of Education and Science (Project FSMR-2024-0003).

Keywords: tactile sensitive element, strain sensor, microcrystalline cellulose, multi-walled carbon nanotubes, composite material.

DOI: 10.61011/TP.2025.03.60867.285-24

Introduction

Tactile perception is an important function of human skin that promotes human interaction with the environment. A human may recognize an object they contact with due to the presence of specialized tactile receptors in their skin, which respond to various external stimuli, such as pressure, bend, strain, temperature change [1,2]. Nevertheless, the tactile sensations may be impaired after skin damage or glove wear, which leads to complications in body management and force application, especially under minor deformations. For example, surgeons are mostly insensitive to soft biological tissues and blood vessels when putting on gloves during a surgery, and cosmonaut's movements are complicated after wearing spacesuits. Electronic skin (e-skin), which has a supersensitive reaction simulating or exceeding the human skin, and is capable of transforming tiny external stimuli into electric signals, is the alternative for the people with impaired sensory perception [3]. Besides, introduction of the tactile feedback may considerably improve the quality of life for people with prostheses, and robotized gripping mechanisms in the surgical facilities may be optimized by the ability to sense when in contact. Therefore, currently the development of various tactile sensors is a relevant task.

The important feature of the flexible composite materials containing carbon nanotubes (CNT), is the acquisition of the piezoresistive property from deformations of CNT in the polymer matrix, which may be the basis for development of the deformation sensors, including strain-sensitive elements in the tactile sensors. This type of sensors has certain advantages. First of all, the presence of exclusive mechanical and electrical properties [4], which provide the sensitivity and strong base for the sensors. Second, they are simple to manufacture, are cost-effective, flexible, their physical parameters (hardness, elasticity etc.) are easy to regulate in a wide range [5].

It was established that CNT have special physical and chemical properties, due to which the materials on their basis achieve more perfect characteristics. For example, when CNT are added to the chitosan matrix in the concentration of ≤ 3 wt.%, the specific electroconductivity of the matrix increases by more than 10 orders, and the low threshold of percolation is achieved at ~ 0.5 wt.% CNT [6]. Besides,

functionalization of CNT with various biomolecules, especially proteins, considerably improves the degree of their biocompatibility. The studies demonstrate practically no cytotoxicity of CNT when used in low concentrations [7–9]. When CNT are added to polymers, nano-composites may be produced with high electroconductivity even at minimum content of CNT, which makes their use economically justified [8–14]. Besides, their ability to form percolation networks capable of self-recovery after the applied deformation, make the nanotubes the ideal candidates for development of highly effective flexible (strain, bend) deformation sensors on their basis [10,15]. To ensure the required flexibility and elasticity, it is effective to apply CNT on the flexible polymer substrates, and to improve the safety of use, the functionalization of nanotubes with proteins and biocompatible components is possible.

It should be noted that the development and implementation of the tactile sensors is a complex task due to the necessity to accurately measure various types of contact forces, which are very weak and may only be sensed by live creatures. In particular, the fingertips and the human tongue are most sensitive, in this case the minimum tactile sensations are the level of pressure $1-2\,\mathrm{mg/mm^2}$ ($10-20\,\mathrm{Pa}$) [16]. It is obvious that the achievement of such sensitivity threshold will make it possible to create the sensitive elements for various types of electronic skin, flexible electronics and tools, including robotics.

This paper studied the layers of the composite material on the basis of the biocompatible microcrystalline cellulose (MCC) and multi-wall carbon nanotubes (MWCNT). The layers were seen as sensitive elements of various forms of deformation, in particular, as a tactile sensitive element (TSE). Their parameters are described in the mode of the tactile deformation sensor prototype, as well as their potential use.

1. Materials, methods of specimen preparation and measurement

Characteristics of the composite material layers within MCC and MWCNT were prepared and studied on the flexible substrates made of polyethylene film (PE — polyethylene).

1.1. Materials

The experiments used to the following materials.

1. MWCNT „Taunite MD“ by LLC „NanoTechCenter“, Russia [17], which were made by method of CVD-synthesis, had the outer diameter of $30-80\,\mathrm{nm}$, inner diameter of $10-20\,\mathrm{nm}$, length of $\geq 20\,\mu\mathrm{m}$, specific surface $\geq 200\,\mathrm{m^2/g}$, pour density $0.03-0.05\,\mathrm{g/cm^3}$ and thermal stability up to 600 °C. In this paper used MWCNT as a filler.

2. MCC ($(C_6H_{10}O_5)_n$, molecular mass 324.3) in the form of a drug from „Evalar“ [18], usually used for losing weight, lessening the appetite, body cleansing, improving gastrointestinal tract function. This drug contains additives (< 1 wt.%), which after decanting remained on the bottom of the vessel, and the supernatant part of the MCC suspension was used as a matrix of a composite material containing the MWCNT filler.

3. PE food wrap from the fresh raw materials was used as a substrate. It had thickness of $30\,\mu\mathrm{m}$. This material has certain useful properties: high strength in the combination with perfect elasticity, low level of water absorption (2 % max), light permeability above 90 %, and also dielectric properties. The wrap inhibits growth of fungi and does not interact with the live organisms, which makes it safe for use. Besides, it has a long service life.

1.2. Preparation of TSE within MCC matrix and MWCNT filler

Prior to the start of the specimen preparation process the aqueous suspensions within 1) MCC, 2) MCC and MWCNT (MCC//MWCNT) were thoroughly mixed using a magnetic mixer for 50 min, then the MCC//MWCNT suspension was dispersed by a strong source of ultrasound (Qsonica Sonicator Q700). One suspension contained 2 wt.% MCC, and the second one — 2 wt.% MCC and 0.8 wt.% MWCNT, the rest is — distilled water.

The aqueous suspension was applied by spraying method onto a flexible substrate from commercial-grade PE (thickness $d_0 \approx 30\,\mu\mathrm{m}$). Besides, the substrates were first treated in various organic solutions (alcohol, acetone) and by ion-plasma beam, which considerably increased their moisture susceptibility. The MCC//MWCNT suspension was applied on the square form of the substrate with side of 20 mm. At the same time the applied suspension layer was exposed to laser radiation to form a dried layer of MCC//MWCNT on the substrate. Laser irradiation is characterized by the following parameters: continuous mode, wavelength 970 nm, radiation capacity $0.003\,\mathrm{W/mm^2}$, radiation time $20-150\,\mathrm{s}$. Upon completion of the preparation process, the substrate together with the applied layer was cut into specimens with width of $w \sim 3-6\,\mathrm{mm}$. Thicknesses d of the applied layers were in the range of $d \sim 0.2-22\,\mu\mathrm{m}$. The specimens had low weight, in particular, a substrate with width of $w = 5\,\mathrm{mm}$ had the mass of $\approx 5\,\mathrm{mg}$, and the layer of the MCC//MWCNT film applied on it with thickness $d \sim 0.23\,\mu\mathrm{m}$, had the estimated mass of $< 10\,\mu\mathrm{g}$. Road map to prepare the specimens of composite material MCC//MWCNT is demonstrated in fig. 1.

1.3. Measurement of certain parameters of specimens

Deformation and measurements of physical parameters of specimens, i.e. TSE, were carried out in a special unit, the operation principle of which is described in [8]. The unit made it possible to measure and automatically save the parameters of resistance, temperature, time, bend angle,

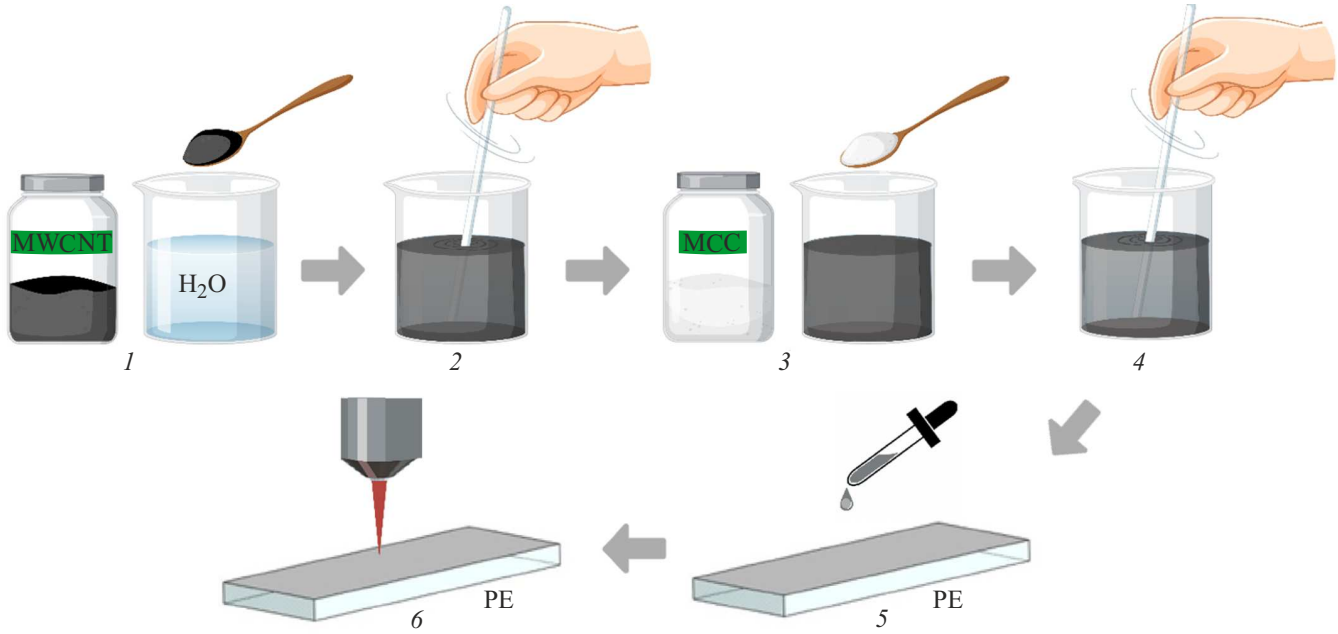

Figure 1. Road map to prepare the specimens of composite material MCC//MWCNT: *1* — aqueous suspension of MWCNT; *2* — magnetic mixing of MWCNT suspension; *3* — aqueous suspension of MCC//MWCNT; *4* — ultrasonic dispersion of aqueous suspension of MCC//MWCNT; *5* — application of aqueous suspension of MCC//MWCNT on PE substrate; *6* — irradiation of MCC//MWCNT layer with laser beam.

number of bend cycles. Bend θ angle varied in the range of $\pm 100°$. TSE deformation sketch is show in fig. 2.

It is thought that at $\theta = 0$ the specimen is not deformed, and at $\theta > 0$ it is deformed (curved in) so that the TSE surfaces come close and at $\theta = +180°$ they are located nearby (fig. 2, *a*). Similarly at $\theta < 0°$ — it is deformed (bent) so that the TSE surfaces drift away from each other, and at $\theta = -180°$ — they are located at the opposite sides (fig. 2, *b*). TSE bending was done in the number of cycles not exceeding 500.

Strain sensibility or strain gauge resistance of the sensor — its response to the deformation that manifests itself in the variation of the active layer resistance. The faster and the more the resistance varies, the higher the strain sensitivity is. Strain gauge resistance of TSE was determined by the ratio to the bend using formula

$$S_\theta = (R_\theta/R_\theta - 1)/\Delta\theta, \qquad (1)$$

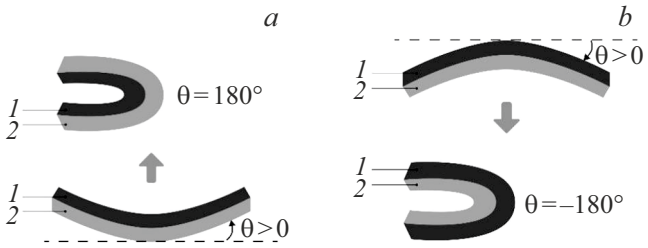

Figure 2. TSE sketch under deformations: *a* — curved in, *b* — bent: *1* — MCC//MWCNT layer, *2* — PE substrate.

where R_θ — resistance in the presence of deformation (bend), R_0 — resistance at the absence of deformation (bend is absent), $\Delta\theta$ — changes of the angle θ.

Electroconductivity of the suspension was measured by the device to assess the water quality AZ8361, and the volume specimens or specimens in the form of the layers — by a multimeter of Agilent 3458A type. Light transmission in the MCC//MWCNT layer in the optical range (wavelength 200–1000 nm) was measured on a spectrophotometer of Genesy suv-vis 10s type.

Images of the specimen microstructure were obtained by the method of scanning electron microscopy using microscope FEI Helios NanoLab. The accelerating voltage was 2 kV, and the electron probe current — 21 pA.

Mechanical parameters were determined using NanoScan 4D unit. It made it possible to measure both nanohardness and modulus of elasticity. The unit automatically measured the parameters in 10 points and provided feedback in the form of their averaged values. The load on the indenter was characterized by value 60 nN, and for the volume specimens of MCC and MCC//MWCNT the Poisson's ratio was deemed to be equal to 0.26.

1.4. Internal structure of the studied specimens

The internal composition of the MCC//MWCNT layers was studied in the cases without laser exposure (fig. 3, *a*) and with laser exposure (fig. 3, *b*). After irradiation with laser, the MWCNT network structure changes. Large clusters (cords from MWCNT) are split into smaller ones,

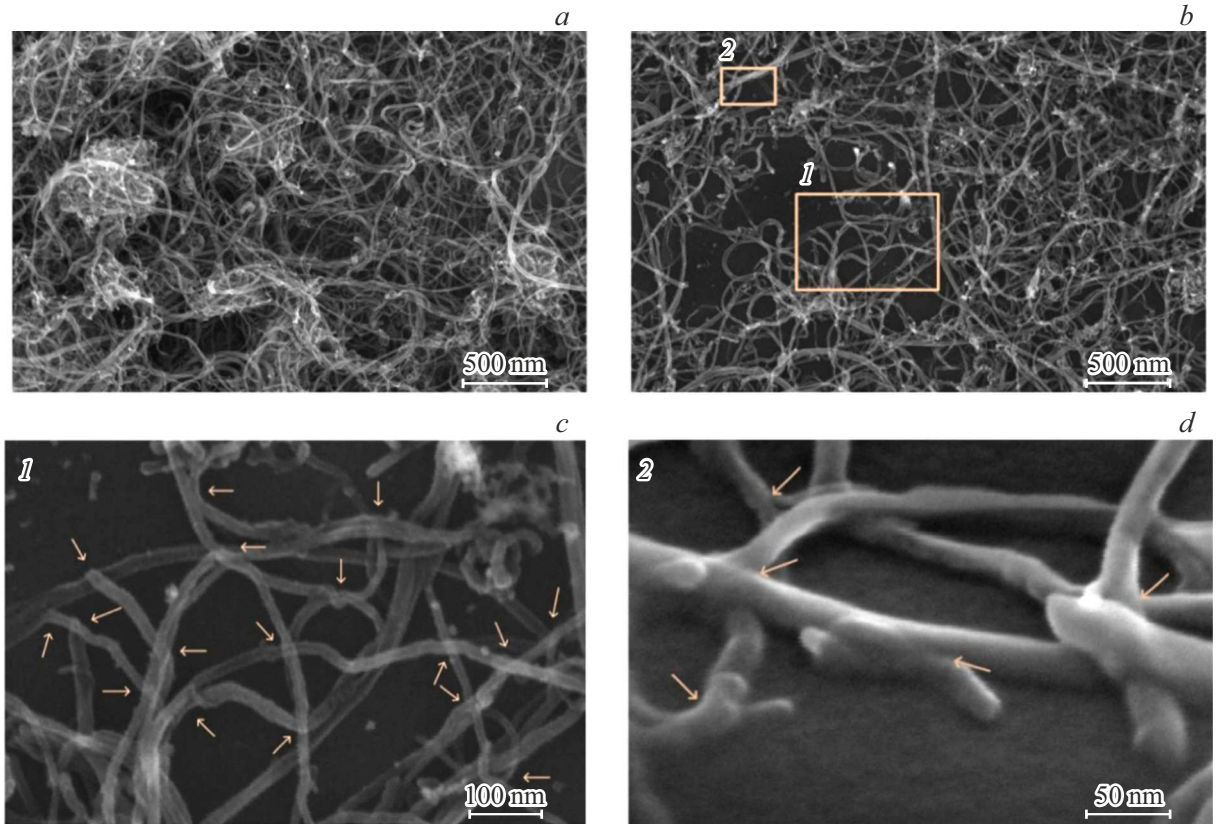

Figure 3. Internal structure of MCC//MWCNT layer made without laser exposure (a) and with laser exposure ($b-d$). The arrows indicate the welded areas of nanotubes formed as a result of laser exposure.

which results in increase of the total number of the clusters and reduction of their average size. The electroconductive MWCNT network after laser exposure acquires a simpler structure, where the areas of nanotube connection prevail. When developing a deformation sensor, it is preferable to use a less dense network, since it provides for lower resistance hysteresis. It is related to the fact that the less dense network extends evenly, and the realignment of the conductive network becomes more stable due to the absence of the high number of the conductive paths. Therefore, the probability of random impact at the conductance from the entangled or randomly joined nanotubes reduces. Fig. 3, *c, d* shows the nanotube welding areas, i.e. additional contacts that are formed under laser exposure. Fig. 3, *c, d* uses arrows to indicate the points of additional contacts between MWCNT. It should be noted that the used parameters of the laser irradiation (see section 2.2), in particular, the absorbed energy, make it possible to weld CNT to each other and form additional contacts between them, which is also demonstrated in other papers [19–21], and may not lead to their damage or ablation, similarly to what happens when exposed to a femtosecond laser at threshold capacities $\geq 13\,\mathrm{MW/mm^2}$ [22].

A multi-angle analyzer of particle size, such as Photocor Complex, was used to estimate the hydrodynamic dimensions of the MCC and CNT polymer particles using the method of dynamic light scattering. MCC particles were characterized by size $500 \pm 200\,\mathrm{nm}$, and after addition of MWCNT and ultrasonic treatment of the suspension their dimensions decreased down to $350 \pm 150\,\mathrm{nm}$. In this case a peak emerged, which is specific for nanotubes, with hydrodynamic size $70 \pm 20\,\mathrm{nm}$, and it is suggested that the nanotubes are not associated with the polymer particles, since their size in the aqueous suspension (without MCC) has approximately the same value.

2. Experimental results and discussion

2.1. Physical and mechanical parameters of TSE

To study the specific electroconductivity σ of TSE, two types of studies were conducted: studies of the aqueous dispersion and dried specimens. The measured data is shown in table 1. You can see that addition of 2 wt.% MCC in the distilled water changes the value σ, and the additional addition of 0.8 wt.% MWCNT increases the suspension electroconductivity again. The other pattern of electroconductivity is observed when dried specimens are measured, which were produced by evaporation of liquid at room temperature.

Table 1. Electroconductivity of aqueous suspensions at temperature 20 °C

Suspensions	σ, mS/m
Distilled water (Distil. water)	0.2
2 wt.% MCC//98 wt.% Distil. water	20
2 wt.% MCC//0.8 wt. MWCNT// 97.2 wt.% Distil. water	90

Note: values σ are given with accuracy of $\pm 5\,\%$

Table 2. Electroconductivity of some volume and film specimens at temperature20 °C

Specimens	σ, S/m
Volume specimen: MCC ($1 \times 5 \times 12$ mm)	$< 10^{-5}$
Volume specimen: 72 wt.% MCC//28 wt.% MWCNT (cylinder — diameter 5 mm, length 12 mm)	2800
Films 72 wt.% MCC//28 wt.% MWCNT with different thicknesses d:	
$0.0225 \times 5 \times 20$ mm	1700 (2.35 kΩ)
$0.0152 \times 5 \times 20$ mm	1570 (2.55 kΩ)
$0.71\,\mu$m $\times$ 5 mm $\times$ 20 mm	1350 (3.0 kΩ)
$0.23\,\mu$m $\times$ 5 mm $\times$ 20 mm	1280 (3.15 kΩ)

Note. Values σ and resistances are given with accuracy $\pm 7\,\%$; at complete loss of moisture the volume specimens of MCC were independently fragmented and converted to the initial powder.

Table 2 presents the typical electroconductivity of volume and film specimens of various composition and shape. According to the data presented in the table, high value of the specific electroconductivity is recorded for the thin films with thickness of $d \approx 0.71$ mm and $0.23\,\mu$m. All film specimens had the same length 20 mm and width in the range of 3–6 mm. The specimens were produced when exposed to laser irradiation, under which the initial values σ increased several times (3–15) relative to the specimens prepared without applying the laser irradiation. Seemingly such behavior is due to the formation of the additional number of contacts between MWCNT, which is noted in section 1.4. The conductance of the volume MCC specimen is practically not recorded, but the volume composite MCC//MWCNT material has the value σ that is 6 orders higher. For the film specimens of the composite material the value σ several times exceeds the volume specimen, despite the fact that the films visually are semi-transparent or well transparent with the visible light transmission coefficient of more than 60 %.

From the data given in table 1 and 2 it is clear that addition of MCC or MWCNT to water at low concentrations substantially varies the specific electroconductivity of the composite material specimens in the forms of aqueous suspension and solid state (dried specimens). It is important that the increase of σ of the suspension is approximately 4.5 times higher after adding MWCNT, i.e. the growth coefficient of value σ is $k_\sigma = 4.5$. The growth is especially drastic in the dried volume specimens, i.e. in them it is $k_\sigma \geq 10^8$. Seemingly, such large spread of values k_σ for the matrices of nanomaterials in the aqueous suspension and volume state correlates with the MWCNT concentration in the matrices. Indeed, in the first case (aqueous dispersion) the matrix includes a filler 0.8 wt.% MWCNT, and in the second case (volume specimens) ~ 28 wt.% MWCNT. Different ratios of MWCNT concentration and MCC matrix in the dried specimens relative to their ratio in the suspensions are caused by the fact that when the suspension specimens are dried, the moisture in them evaporates nearly fully, and the composition of the volume specimen has approximately the following ratios: MWCNT $\sim 28\,\%$ and MCC $\sim 72\,\%$. Here the initial concentrations in the aqueous suspension are taken into account: 2 wt.% MCC and 0.8 wt.% MWCNT. The significant difference of coefficients k_σ in the suspension (~ 4.5) and dried specimens ($\geq 10^8$) is caused by the significant difference of MWCNT concentration in them. Indeed, the corresponding MWCNT concentrations differ significantly from the threshold value ≥ 2 wt.% MWCNT at the start of the percolation mechanism of electroconductivity in the composite materials containing CNT [23]. In the aqueous suspension the concentration of MWCNT 0.8 wt.% is significantly lower than the threshold concentration of

Table 3. Mechanical parameters of dried specimens at temperature 20 °C

Specimens	ρ, g/cm^3	H_v, GPa	E, GPa
100 wt.% MCC	1.35 ± 0.01	0.13 ± 0.02	1.8 ± 0.3
72 wt.% MCC//28 wt.% MWCNT	1.51 ± 0.01	0.25 ± 0.04	5.9 ± 1.2

2 wt.%, and in the dried specimens 28 wt.% MWCNT is much higher. For the last case the coefficient k_σ increases substantially in the film specimens due to laser exposure they are subjected to, and additional number of contacts are formed between CNT, which was noted above.

The studies of the mechanical parameters of solid specimens also demonstrated their substantial changes, when the MWCNT filler was added to their matrix. Table 3 presents the measured values of density ρ, Vickers hardness H_v and Young's modulus E. You can see that the MWCNT filler considerably increases the parameters of the matrix, for example, coefficients to increase k_ρ, k_H and k_E, density, hardness and Young's modulus, which are accordingly equal to 1.12, 1.92 and 3.34. The values of coefficients k_ρ, k_H and $k_E > 1$ mean the impact of the MWCNT filler on the matrix parameters. Note that parameter ρ for MCC is usually ~ 1.54 g/cm^3, however, for the dried specimens of MCC ρ it was 1.35 g/cm^3. This indicates the porosity of the MCC matrix and reduction in its porosity degree when using the MWCNT filler or single-walled CNT, which was also noted in papers [14,24]. They used as a matrix a bovine serum albumin, carboxymethylcellulose, collagen and other biological materials or their systems.

2.2. Strain-sensitive characteristics of TSE

Fig. 4 shows the dependences of the relative resistance of the specimens on the bend angle, i.e. $R(\theta)/R_0$, where the quantity of the measurement cycle $n = 1$, R_0 — resistance at $\theta = 0$, and the designations with the markers are provided: continuous line — film $d = 0.23\,\mu$m, $R_0 \approx 3.15$ kΩ; dashed line — layer $d \sim 15\,\mu$m, $R_0 \approx 2.55$ kΩ. Dependences $R(\theta)/R_0$ vary significantly among each other at various thicknesses of TSE. For example, for a thin film ($d \approx 0.23\,\mu$m) the behavior $R(\theta)/R_0$ is approximately linear, while for a thick layer ($d \approx 15.2\,\mu$m) this dependence is similar to a turned over parabola with maximum at $\theta = 0$. These curves also differ by the fact that in the first case the hysteresis is $R(\theta)/R_0$ smaller than in the second case.

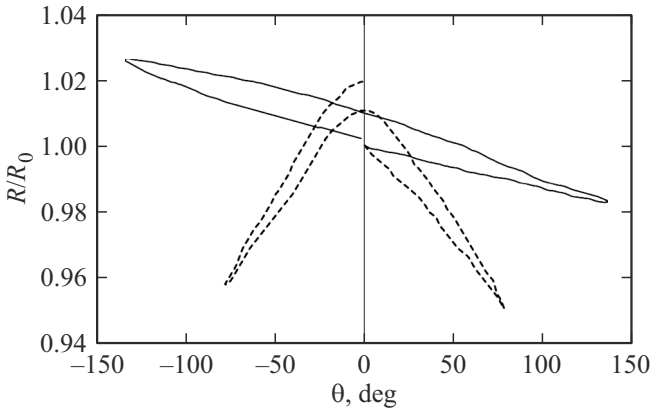

Figure 4. Typical dependences for some films at the first measurement cycle $n = 1$: continuous line — film $d = 0.23\,\mu$m, dashed line — layer $d \sim 15.2\,\mu$m.

Quantitative value of hysteresis at $R(\theta)$ with fixed θ was estimated as

$$h_R = 2(R_{\max} - R_{\min})/(R_{\max} + R_{\min}), \qquad (2)$$

where ($R_{\max}$, $R_{\min}$ — maximum and minimum values of TSE resistance. The following is specific for $R(\theta)$: hysteresis has the maximum value of ($h_R \leq 2\,\%$) during the first cycle of measurement, and as the quantity n increases, the value h_R decreases; simultaneously the resistance of TSE and its strain sensitivity coefficient S_θ, i.e. slope $R(\theta)$ increases: $S_\theta = (1/R)dR/d\theta$, determined according to (1). For example, for a specimen with thickness of $d = 0.23\,\mu$m at $n = 1$ the value S_θ (fig. 5) is approximately equal to 0.036 %/deg, and at $n = 100$ — $S_\theta \sim 0.223$ %/deg. Linear dependence R on θ both at $\theta > 0$ and at $\theta < 0$ means that TSE is sensitive to various forms of bend shown in fig. 2. Practically linear dependence $R(\theta)$ in the entire range of the bend angle variation means that in the area $\theta = 0{-}66°$ this film reacts to the bend of „curved in“ type, according to fig. 2, *a*, and in the area $\theta = -66°{-}0$ — to the bend of „bent“ type according to fig. 2, *b*. Therefore, the behavior of this TSE is similar to a bipolar deformation sensor, which is sensitive both to deformation and deformation type [11]. Such bipolar behavior is specific only for thin films with thickness $d < 1\,\mu$m, while for thick films $d \geq 10\,\mu$m the unipolar behavior is specific in the entire range of bend (fig. 4, $d \sim 15.2\,\mu$m). In this case as angle θ of any polarity increases. the measured resistance always decreases, and at $\theta = 0$ the dependence $R(\theta)$ has maximum. Besides, the implemented low value of strain sensitivity $S_\theta \approx 0.19$ %/deg ($n = 100$) and high value $h_R \sim 4\,\%$, are practically 2 times different from the corresponding parameters for the thin film case. In general, based on the positive readings (high S_θ and low h_R), the TSE based on a thick layer is inferior to the TSE based on a thin layer.

Significant difference in the TSE behavior within MCC//MWCNT at different thicknesses of its layers may be explained by sketches given in fig. 5.

For a thin film (fig. 5, *a, b*) CNT are a single layer. For deformation of „curved in“ type, MWCNT get closer to

each other, which increases the density of the contacts between them and decreases the electric resistance. In case of „curved in“ type deformation, CNT move away from each other, which decreases the density of the contacts and accordingly increases the electrical resistance of the MCC//MWCNT layer. Such behavior is correlated approximately by the linear dependence R on θ, which is observed in the experiment.

At any type of deformation („curved in“, „bent“), the thick layer (fig. 5, *c, d*) is seen as a combination of several layers made of CNT. In process of deformation some of these layers get closer, while others move away from each other. Therefore, for one group of layers there is a decrease in the electrical resistance, while for the other group of MWCNT it increases. The general resistance is registered on the contact sites of the device, which arises as a result of interaction of these MWCNT layers. One may assume the corresponding changes in the resistance of the layers as $R_1 = R_0(1 - \alpha\theta)$ and $R_2 = R_0(1 - \alpha\theta)$, where R_0 — resistance to bend of layers, θ — bend angle, R_1, R_2 — suggested resistances of layers, α — parameter. Full resistance R will be as parallel connection of R_1 and R_2 i.e.

$$R = R_0\left[1 - (\alpha\theta)^2\right]. \tag{3}$$

You can see that full resistance of the layer is an even function and does not depend on the sign θ, dependence R on θ has the shape of parabola, which corresponds to the experimental result obtained for the TSE prototype based on the thick layer from the MCC//MWCNT composite material.

According to fig. 5, for TSE based on the thin film between R and θ the relation is negative, i.e. the resistance decreases as the bend angle or deformation value increases. This makes it possible to use the sensor in the feedback systems, for example, to hold the bend angle (deformation) at the specified level.

Fig. 6 shows a specimen (thin layer — $d \sim 0.71\,\mu$m) of the MCC//MWCNT composite material on the PE substrate without deformation and with deformation under load.

With account of the film parameters, the value S_θ, the mass of the weight m and its dimensions, the bend depth h and the corresponding bend angle, the minimum registered

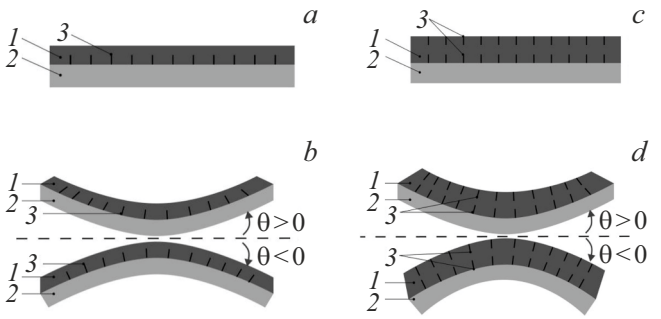

Figure 5. Sketch of TSE prototype structure: *a, c* — layers without deformation; *b, d* — layers after deformation. *1* — MCC//MWCNT layers, *2* — substrate, *3* — MWCNT. Layer thickness scales are not observed.

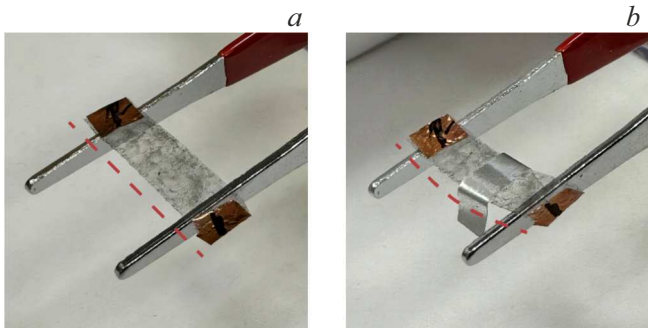

Figure 6. TSE prototype: layer $d \sim 0.71\,\mu$m on PE substrate $d_0 = 30\,\mu$m: *a* — without bend; *b* — bend under weight $m = 50$ mg.

pressure P is detected using the given TSE. The following data were used: $l = 14$ mm — length of the film between the supports, $h \approx 2$ mm, $S_\theta \approx 0.19$ %/deg, $m = 50$ mg and the area of TSE coverage with the weight 20 mm^2, the change of the resistance was obtained by ~ 1.66 %, and pressure $P \sim 5$ mg/mm^2 (~ 50 Pa) was registered. Since the measurement accuracy 0.05–0.1 % is acceptable for a strain gage, one may presume that the analyzed TSE may record pressure ≤ 0.2 mg/mm^2 (≤ 2 Pa). This means the possibility to fix the lumps (state of „bent“) or indents (state of „curved in“) on the surface of the study item, which have the height or depth values of around $h \leq 50\,\mu$m.

Fig. 7 shows photos of TSE in the loaded and unloaded states. The specimen (thin layer — $d \sim 0.23\,\mu$m) is fixed with one end, and the load is fixed on the free end. The load was a copper foil with the following parameters: 1×4 mm; mass 0.6 mg, and TSE was bent at values $l \approx 12$ mm, $h \approx 2.5$ mm, $\theta \approx 11°$. Change in the TSE resistance when bent by 11° corresponds to registration of 1.5 Pa pressure.

Therefore, the registered or estimated P and h of the specimens are comparable to the tactile sensitivity of human fingers or tongue (~ 2 mg/mm^2) [25].

It should be noted that the MCC//MWCNT layers applied on the substrate are partially heterogeneous by thickness. Seemingly it is caused by the rough PE surface and the inability to provide complete hydrophilic behavior, which significantly impacts the thickness homogeneity of the MCC//MWCNT layers applied on the substrate. However, these layers show high values of strain sensitivity and stability at their multiple bend cycles and when stored in the room conditions for five years. In the last case the value S_θ varied in the range of $< \pm 20$ % of the initial value. The best stable values of parameters are maintained for the thin layers ($d \leq 1\,\mu$m).

For the human soft tissue the Young's modulus $E < 0.5$ MPa and for use of PE in the medicine, its value E must be characterized by a smaller or similar order. The full modulus of elasticity E_s of the PE structure includes the modulus of elasticity E_0 of the substrate and modulus of elasticity E of the PE layer. When the tactile sensor is located as shown in fig. 6 (fixed on ends), or when fixed

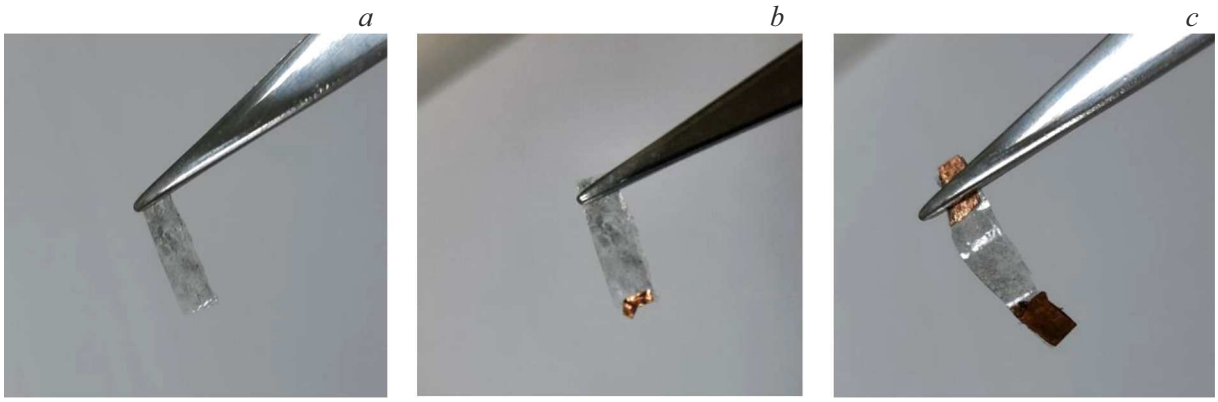

Figure 7. TSE prototype: layer $d \sim 0.23\,\mu$m on PE substrate $d_0 = 30\,\mu$m: *a* — without bend; *b* — bend under weight. Load $m = 0.5$ mg is applied to the end of the film, *c* — load $m = 5.5$ mg is applied to the end of the film.

with one end only (fig. 7), the corresponding values E_s may be assessed as

$$E_s \sim \frac{E_0 d_0 + E d}{d_0 + d}, \tag{4}$$

$$E_s \sim \frac{E_0 d_0^3 + E d^3}{(d_0 + d)^3}. \tag{5}$$

The estimates used the known values of the PE substrate parameters [26]: $E_0 = 200$ MPa, $d_0 = 30\,\mu$m, and the measured parameters, according to table 3: $E = 5.87$ GPa, $d = 0.23\,\mu$m. Numerical values E_s of the tactile sensor change by less than 12% relative to the value E_0 for the substrate according to (4), and less than by 1% for the case (5). Therefore, adding MWCNT to the MCC matrix increases many parameters of the matrix (all coefficients k_σ, k_ρ, k_H and $k_E > 1$), however, increase of E practically does not impact the value E_s in case of the thin layer of TSE ($d \leq 1\,\mu$m). Therefore, the smaller is the ratio between the thicknesses of TSE and the substrate, the lower is the full hardness of the MCC//MWCNT//substrate structure. This correlates with the position necessary to control deformation of the human soft tissues.

The studied layers of TSE ($d \leq 1\,\mu$m) are semi-transparent. Their light transmission T relative to the PE substrate in the range of wavelengths 300−1000 nm reaches 61−74% for the layer $d \approx 0.23\,\mu$m, and for the layer $d \approx 0.71\,\mu$m — 48−62%. As the wavelength increases in the range 400−700 nm the value T grows linearly, which is specific for the biological materials, such as MCC in the matrix of the MCC//MWCNT composite material.

Conclusion

It is important to review the prospects of potential use of the studied layers, some examples of which are given below.

1. The studied layers of the MCC//MWCNT composite material may be seen as the main parts of the TSE in the tactile deformation sensor. They have advantages relative to the known tactile deformation sensors to develop a tactile matrix [27]: simple to make, wide dynamic range of bend angle variation, bipolarity of deformation registration, possibility to minituarize the geometric dimensions of the TSE to the submillimeter or micron dimensions (scaling), and regulation depending on the purpose of using the tactile sensor characteristics, in particular: tactile sensitivity values, relaxation time, specific electroconductivity, moduli of elasticity etc. The TSE parameters may be changed by modifying the concentration of the MWCNT filler, the laser irradiation capacity, weight and dimensions of the sensor elements or selection of the substrate parameters.

2. The studied films of the MCC//MWCNT composite material demonstrated high specific electroconductivity ($\sim 10^3$ S/m) at layer thickness $\leq 1\,\mu$m. The layers are formed by application of the aqueous suspension of the MCC//MWCNT composite material on the substrate with further exposure to the laser irradiation.

3. Laser exposure of the materials with the purpose to change their characteristics, as the process method is simple to implement and may be used widely, for example, in the flexible electronics or the systems, which require electroconductive structures, which do not contain metal elements. For example, using the MCC//MWCNT layers when substituting the electrodes from noble metals (Au, Pt etc.) in a high-field actuator [2], or in a low-field actuator-implant to eliminate the upper eyelid lowering [28]. It is evident that the specified substitution will make it possib;e to considerably improve the flexibility of the electrodes and the efficiency of the actuator operation.

Decrease in the thickness of the MCC//MWCNT composite material layers and improvement of the technology for their application on the substrate will make it possible to a larger extent to improve its flexibility and optical transparency to the acceptable threshold ≥ 85%. Therefore, this will expand its application in various areas of the flexible electronics, for example, in „smart glass“ type actuators — which take the flat, wavy or opaque form to transmit, distort or restrict the image, accordingly [29].

The flexible electronics also values the surface density of the transparent layer, in the case of the thin layers studied in the paper ($\leq 14\,\mu$m) it is $< 300\,\text{mg/m}^2$ (estimated) at transparency $T \geq 74\,\%$. These values are more optimal that $160-780\,\text{mg/m}^2$ and $T \sim 65\,\%$ for the films from the silver nanofibers actively developed at the moment [30].

4. Working on the capabilities of the MCC//MWCNT composite material layers will make it possible to develop electronic skin (e-skin) on their basis, which is currently developed on the basis of the nanomaterials containing CNT or graphenes [31,32]. To achieve this goal, high-sensitivity tactile-sensitive elements of submillimeter micron size will be necessary. Currently the studies are in progress in this area, and supersensitive elements have already been developed, which may record the minimum pressure at the level 1.37 Pa [33]. We also studied the MCC//MWCNT layers that make it possible to record the minimum pressure at the level of around 2 Pa.

When scaling the structure that we proposed to the required level, it is possible to develop miniature T-sensors for 2*D*-electronic skin with various receptors similar to those that were proposed in source [34].

5. The high-sensitive TSE based on the studied MCC//MWCNT films may be used in the low-invasive surgery to increase the contact sensitivity of various tools, and also in a medical endoscope to determine the pressure or state of the tissue, including masses without a biopsy by the analysis of their elasticity or other mechanical properties [35].

Acknowledgments

The authors express gratitude to employees A.G. Markov, A.V. Kuksin, D.T. Murashko, P.N. Vasilevsky for their assistance in doing the experiments.

Funding

The work was performed under the state assignment of the Ministry of Education and Science of Russia (Project FSMR-2024-0003).

Conflict of interest

The authors declare that they have no conflict of interest.

References

[1] A. Salim, S. Lim. Sensors, **17**, 2593 (2017). DOI: 10.3390/s17112593
[2] S. Chun, I. Hwang, W. Son, J.H. Chang, W. Park. Nanoscale, **10**, 10545 (2018). DOI: 10.1039/C8NR00595H
[3] A. Chortos, L. Jia, Z. Bao. Nat. Mater., **15** (9), 937 (2016). DOI: 10.1038/nmat4671
[4] N. Hu, H. Fukunaga, S. Atobe, Y. Liu, J. Li. Sensors, **11** (11), 10691 (2011). DOI: 10.3390/s111110691
[5] Y. Miao, L. Chen, R. Sammynaiken, Y. Lin, W.J. Zhang. Rev. Sci. Instrum., **82** (12), 126104 (2011). DOI: 10.1063/1.3665959
[6] A.M. Kamalov, V.V. Kodolova-Chukhontseva, E.N. Dresvyanina, T.P. Maslennikova, I.P. Dobrovolskaya, E.M. Ivankova, E.N. Popova, V.E. Smirnova, V.E. Yudin. ZhTF, **92** (3), 435 (2022) (in Russian). DOI: 10.21883/JTF.2022.03.52138.278-21
[7] M. Chu, H.E. Naguib. Smart Mater. Struct., **30** (6), 065003 (2021). DOI: 10.1088/1361-665X/abefb6
[8] L.P. Ichkitidze, A.Y. Gerasimenko, V.M. Podgaetsky, S.V. Selishchev. Mater. Phys. Mech., **37**, 153 (2018).
[9] G.A. Timerbulatova, P.D. Dunaev, L.M. Fatkhudinova. Meditsina truda i promyshlennaya ekologiya, **59** (9), 770 (2019) (in Russian). https://doi.org/10.31089/1026-9428-2019-59-9-770-771
[10] S. Jung, H.W. Choi, F.C. Mocanu, D.W. Shin, M.F. Chowdhury, S.D. Han, J.M. Kim. Sci. Rep., **9** (1), 1 (2019). DOI: 10.1038/s41598-018-37219-w
[11] L.P. Ichkitidze, V.A. Petukhov, A.Yu. Gerasimenko, V.M. Podgaetsky, S.V. Selischev. Patent № 2662060 C1
[12] M. Chu, H.E. Naguib. Smart Mater. Struct., **30** (6), 065003 (2021). DOI: 10.1088/1361-665X/abefb6
[13] A. Markov, R. Wördenweber, L. Ichkitidze, A. Gerasimenko, U. Kurilova, I. Suetina, M. Mezentseva, A. Offenhäusser, D. Telyshev. Nanomaterials, **10**, 2492 (2020). DOI: 10.3390/nano10122492
[14] L. Ichkitidze, A. Gerasimenko, D. Telyshev, V. Petukhov, E. Kitsyuk, V. Podgaetsky, S. Selishchev. In: Proceed. Intern. Conf. on „Physics and Mechanics of New Materials and Their Applications“ PHENMA 2018. Springer Nature Switzerland AG ed. by I.A. Parinov (Springer Proceed. in Physics, 2019), p. 523–535. DOI: 10.1007/978-3-030-19894-7_40
[15] A. Salim, S. Lim. Sensors, **17**, 2593 (2017). DOI: 10.3390/s17112593
[16] A.V. Litvinov. *Norma v meditsinskoy praktike*: sprav. posobie, pod red. A.V. Litvinova (MEDpress-inform, M., 2016), s. 144 (in Russian).
[17] Electronic source. Available at: URL: https://zavkom.com/otrasli/drugie-otrasli/ (date of access: 14.07.2024)
[18] Electronic source. Available at: URL: https://shop.evalar.ru/catalog/ (date of access: 14.07.2024)
[19] J. Chrzanowska, J. Hoffman, A. Małolepszy, M. Mazurkiewicz, T.A. Kowalewski, Z. Szymanski, L. Stobinski. Phys. Status Solidi, **252** (8), 1860 (2015). DOI: 10.1002/pssb.201451614
[20] A.Y. Gerasimenko, O.E. Glukhova, M.S. Savelyev. JPCS, **1134**, 012016 (2018). DOI: 10.1088/1742-6596/1134/1/012016
[21] Y. Yanping, C. Jimin. Laser Phys. Lett., **13** (6), Art.066001 (2016). DOI:10.1088/1612-201/13/6/066001.
[22] C. Kocabas, M.A. Meitl, A. Gaur, M. Shim, J.A. Rogers. Nano Lett., **4** (12), 2421 (2004). DOI: 10.1021/nl048487n
[23] L.P. Ichkitidze, O.E. Glukhova, G.V. Savostyanov, A.Yu. Gerasimenko, V.M. Podgaetsky, S.V. Selishchev. Proceed. of SPIE–The Intern. Society for Optical Eng., **10685**, 106853Q (2018). DOI: 10.1117/12.2306812
[24] L.P. Ichkitidze, A.Yu. Gerasimenko, V.M. Podgaetsky, S.V. Selishchev, A.A. Dudin, A.A. Pavlov. Mater. Phys. Mech., **37** (2), 140 (2018).
[25] I.A. Tarasenko, G.A. Piyavchenko, E.V. Mityaeva. Zhurnal nauchnykh statey „Zdorovie i obrazovanie v XXI veke“ (Seriya meditsina) **14** (2), 57 (2012) (in Russian).

[26] Electronic source. Available at: URL: https://plastinfo.ru/information/articles/42/ (date of access: 14.07.2024)
[27] J. Park, B. Seo, Y. Jeong, I. Park. Adv. Sci. (Weinh), **11** (20), e2307427 (2024). DOI: 10.1002/advs.202307427
[28] S.S. Hosseini, B. Yamini, L. Ichkitidze, M. Asadi, J. Fernandez, S. Gholampour. Nanomater., **13**, 473 (2023). DOI: 10.3390/nano13030473
[29] D. Friemert, C. Terschüren, B. Groß, R. Herold, N. Leuthner, C. Braun, U. Hartmann, V. Harth. In: Digital Human Modeling and Applications in Health, Safety, Ergonomics and Risk Management. Human Communication, Organization and Work: 11th International Conference, DHM 2020, Held as Part of the 22nd HCI International Conference, HCII 2020, Copenhagen, DenmarkProceedings, Part II 22 (2020). DOI: 10.1007/978-3-030-49907-5_25
[30] S. Shian, R.M. Diebold, A. McNamara, D.R. Clarke. Appl. Phys. Lett., **101**, 061101 (2012). DOI: 10.1063/1.4742889
[31] K.-S. Sohn, J. Chung, M.-Y. Cho, S. Timilsina, W.B. Park, M. Pyo, N. Shin, K. Sohn, J.S. Kim. Sci. Rep., **7**, 11061 (2017). DOI: 10.1038/s41598-017-11663-6
[32] P. Miao, J. Wang, C. Zhang, M. Sun, S. Cheng, H. Liu. Nano-Micro Lett., **11** (1), 71 (2019). DOI: 10.1007/s40820-019-0302-0
[33] G. Wu, X. Li, R. Bao, C. Pan. Adv. Funct. Mater., **36** (21), 2313857 (2024). DOI: 10.1002/adma.202313857
[34] C. Chen, F.Q. Xu, Y. Wu, X.L. Li, J.L. Xu, B. Zhao, Z. He, J. Yang, W. Zhang, J.W. Liu. Adv. Mater., **36**, 25 (2024). DOI: 10.1002/adma.202400020
[35] D.V. Gusev, N.L. Danilova, R.S. Litvinenko, Yu.A. Mikhailov, V.V. Pankov, V.S. Sukhanov. Izvestiya VUZ, Elektronika, **20** (5), 511 (2015) (in Russian).

Translated by M.Verenikina